Towards characterizing and reducing artifacts caused by varying projection truncation

Borg, Leise; Jørgensen, Jakob Sauer; Sporring, Jon

Publication date:
2017

Document Version
Publisher's PDF, also known as Version of record

Towards characterizing and reducing artifacts caused by varying projection truncation

Borg, Leise; Jørgensen, Jakob Sauer; Sporring, Jon

Towards characterizing and reducing artifacts caused by varying projection truncation

Leise Borg[1], Jakob Sauer Jørgensen[2], Jon Sporring[1]

[1] *Image section, Department of Computer Science, University of Copenhagen, Denmark*

[2] *Department of Applied Mathematics and Computer Science, Technical University of Denmark, Denmark*

February 24, 2017

Contents

1 Background

This report documents the work done on a special limited-angle tomographic reconstruction problem for the P^3-project.

The data is achieved (for the Cinema-project) at the SPring-8 synchrotron facilities in Japan by a monochromatic, parallel-beam setup. We use data from "wetscan01". For acquisition of data, a chalk sample is irradiated by X-rays by known intensity at angles uniformly and closely spaced, covering 180 degrees. The X-ray intensities are measured after passing through the sample. In this case, data is not fully available for all angles: For some angles, the measurements are completely absent and for other angles, the measurements are partly absent. Problems where data is completely absent in certain angular ranges, are typically termed limited-angle (LA) problems, and are in general well understood. This case, however, is a special LA (sLA) problem (see Sections 1.1 and 1.2 for details).

From the data, a reconstruction of the material-specific X-ray attenuation coefficient across the sample, can be obtained by means of several types of reconstruction methods. At the synchrotron site, they provide a reconstruction, based on some type of a filtered back-projectection (FBP) method. The reconstructions contain artifacts, and we suspect these artifacts to be caused by the patterns of the missing data in the sinogram. A first, naïve FBP-based reconstruction from the available data is calculated. This reconstruction contains artifacts resembling the artifacts in the reconstruction provided by the synchrotron facilities. The purpose of this work is to find methods that can reduce the artifacts.

We are aware that other types of reconstruction methods can be used, such as algebraic methods. This work investigates, however, only FBP as a reconstruction method, in combination with preprocessing of the data.

1.1 Experimental set-up causing truncated projections

Viewing the interior of chalk samples of size 1-2 mm at different time instances, makes it possible to predict petrophysical parameters and how they change in time. This is useful when searching for oil in the North Sea. A percolation cell is developed for handling high temperature and pressure when the chalk samples are subjected to a fluid flow through their pores. It contains four metal bars which shadow for the signal in certain angles, as seen in Figure 1.

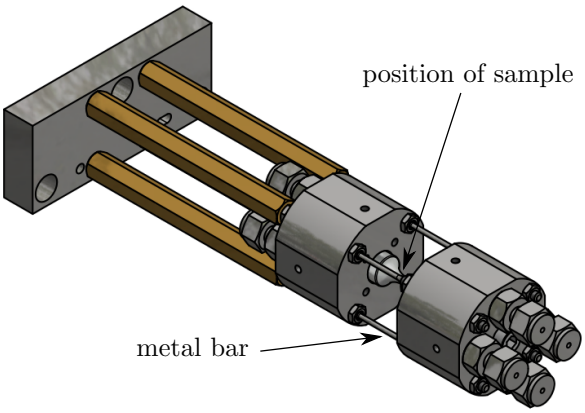

Figure 1: *The percolation cell.*

For a parallel beam, this means that for specific angles, the bars hinder the X-rays to reach the detector, and no signal is recorded at the detector array. This set-up us sketched in Figure 2a. Here, we see that for some angles there is full signal and at other angles there is no signal. The transition between the two situations - "signal" and "no signal" - does not happen in one step. To illustrate this, an intermidiate step is shown in Figure 2b. Here, two bars block the outermost rays of the projection, and only the center rays reach the detector. The fraction of the beam that reaches the detector becomes smaller and smaller as we move towards the "no signal" situation. We could say that when moving from "signal" to "no signal", the effective detector width decreases, resulting in truncated projections, until the metal bars block the beam entirely.

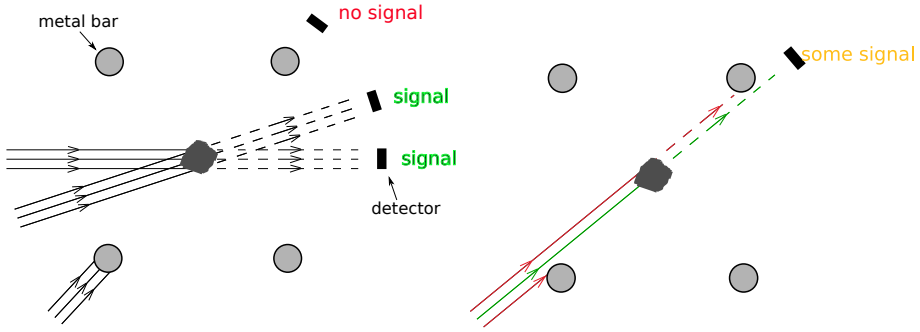

(a) *For some angles no signal is recorded at the detector.* (b) *The effective detector width decreases when moving from "signal" to "no signal".*

Figure 2: *A sketch of the experimental parallel-beam set-up.*

At the synchrotron site, they provide a reconstruction based on filtered back-projection (FBP). We do not know how they have implemented the method, but

they do take into consideration region-of-interest effects (see Section 1.2.2. This reconstruction and three zooms are shown in Figure 3. The reconstruction contains artifacts; Streaks are carving through the image with angles of about 45 and 135 degrees and are rather profound away from the image center. This makes it difficult to segment the pore structures to be used for predicting the petrophysical parameters of the chalk sample. We want to find a method that does not give streaks in the reconstruction.

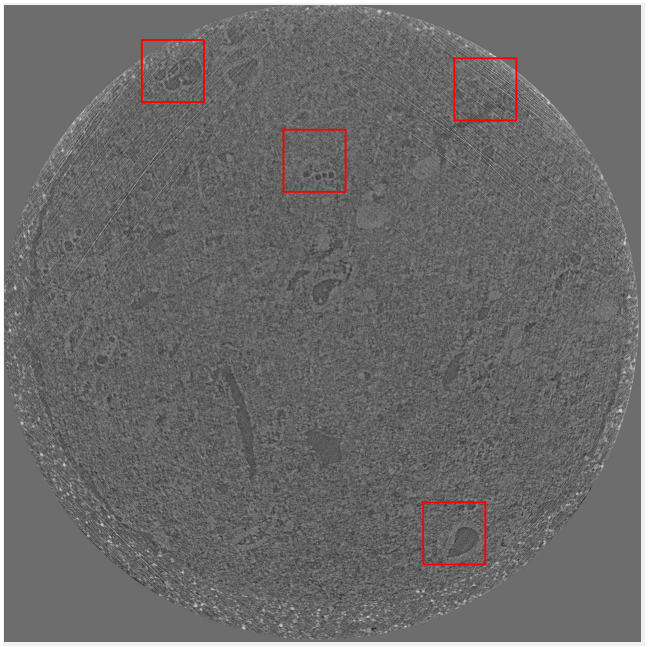

(a) *Reconstruction*

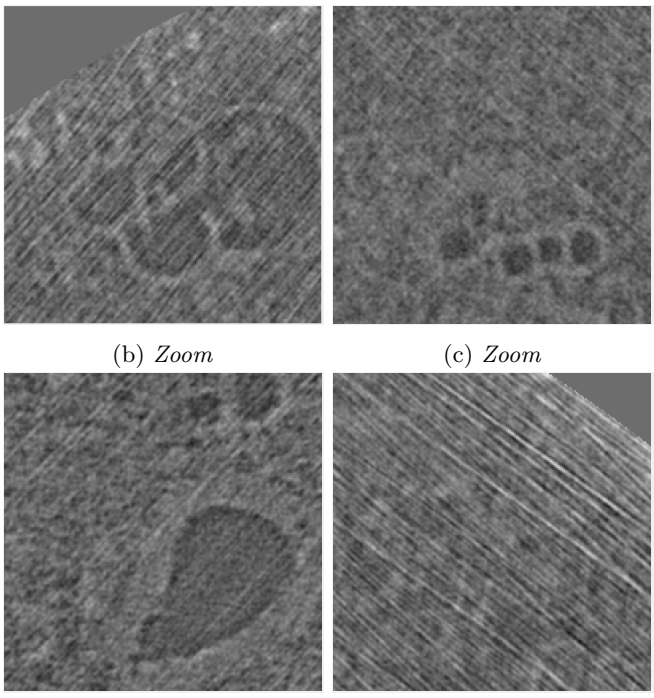

(b) *Zoom* (c) *Zoom*

(d) *Zoom* (e) *Zoom*

Figure 3: *An FBP-based reconstruction provided by the acquisition site.*

1.2 Data: From raw transmissions to a segmented sinogram

1.2.1 Forming the sinogram

As a consequence of the acquisition set-up, the recorded 2D transmissions are truncated for certain angles. In Figure 4, transmissions are shown for six measurement angles numbers, a: 438, 442, 446, 459, 454, and 462 out of $a_{\max} = 1800$ measurements, covering 180 degrees. The transmissions show the case when moving from "full signal" (transmission 438), via "some signal" (transmissions from 442-454) to "no signal" (transmission 462).

The data is provided as relative transmission values and are already corrected for dark and white fields:

$$t_{\text{corrected}}(x) = \frac{t_{\text{raw}} - t_{\text{dark}}}{t_{\text{white}} - t_{\text{dark}}}, \tag{1}$$

where

$$t_{\text{white}} = (a_{\max} - a) \cdot t_{\text{white\_before}} + a \cdot t_{\text{white\_after}}. \tag{2}$$

The dark field, denoted t_{dark}, is a measurement in absence of beam, the white field, t_{white}, is a measurement in the presence of a beam but without the sample, and the raw data, t_{raw}, is the data measured in the presence of a beam and an object. The white field was measured before, $t_{\text{white\_before}}$, and after, $t_{\text{white\_after}}$, measuring t_{raw}, as the detector sensitivity might change over time during the data acquisition. Therefore, equation 2 is a weighted average of the white field before and after the data acquisition.

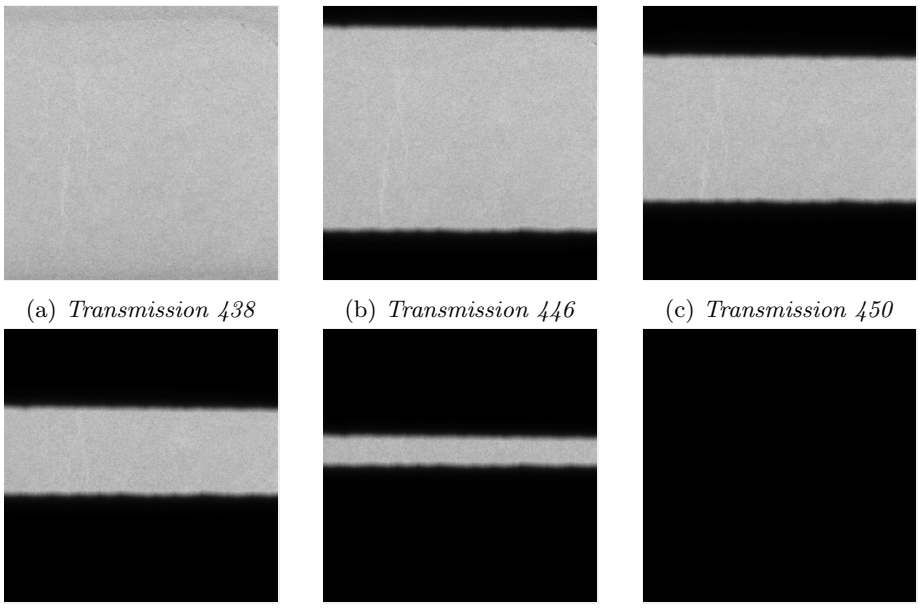

(a) *Transmission 438* (b) *Transmission 446* (c) *Transmission 450*

(d) *Transmission 454* (e) *Transmission 458* (f) *Transmission 462*

Figure 4: *A range of 2D transmissions, $t_{corrected}$, corrected for dark and white field*

Picking out columns number 1000 (approximately the ones in the middle) of all 1800 transmissions, and collecting them side-by-side, yields a tranmission sinogram, $T_{\text{corrected}}$, for slice number 1000 of the object to be imaged. Because the transmissions miss signal for specific angles, the corresponding transmission sinogram, contains zeros in certain areas, as shown in Figure 5. The range of the sinogram is between 0 and 0.53 and denotes the fraction of photons detected out of the emitted photons. Each transmission slice (one for each angle) appear as a column in the transmission sinogram, and therefore we have ϕ, on the abcissa, representing the projection angle number covering 180 degrees with 1800 columns. The detector displacement (or detector width), s, is on the ordinate.

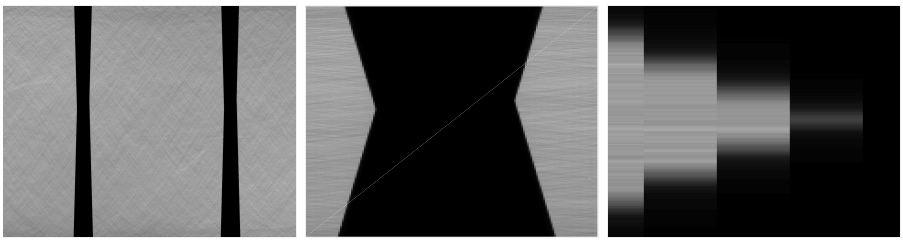

(a) *Full transm. sinogram* (b) *Zoom* (c) *Zoom of zoom*

Figure 5: *Transmission sinogram,* $T_{corrected} \in [0, 0.53]$.

The sinogram resembles a limited-angle (LA) problem, with clean angular data cut-offs. However, it is not exactly the case, since truncated projections are present, as seen in the zooms in Figures 5a and 5c. This is due to the transition situation where only a part of the beam reaches the detector array, as showed in Figure 2b. This results in a staircasing effect with discontinuous boundaries in the angular direction caused by discretization of the angular displacement. The smooth transition across the truncated projections is probably due to partial penetration of the X-rays through the metal bars.

1.2.2 Region-of-interest

The problem we are working on is a region-of-interest (ROI) problem, also known as an interior problem: The detector array width is smaller than the width of the sample, meaning that the object is not covered entirely by the beam. It is known mathematically that ROI data is not sufficient to determine a unique solution [2], and both analytic and algebraic reconstruction methods will suffer from artifacts. The artifacts appear as a bright circle surrounding the region of interest and higher pixels values inside the region, which falls off as moving towards the ROI center. There do exist means to improve image quality for ROI-problems such as padding in the sinogram or adding specific priors in the algebraic models.

1.2.3 Metal segmentation

According to Lambert-Beer's law of attenuation, we must take the negative logarithm of the transmission sinogram, $T_{\text{corrected}}$, to obtain the regular sinogram, I:

$$S = -\log(T_{\text{corrected}})$$

However, missing transmissions occur as zeros, yielding plus infinity after negative logarithm. Also, since the transition between "signal" and "no signal" is smooth, there will appear near-to-zero values, yeilding very large positive values after negative logarithm. The pixel with near-to-zero values only appear next to pixels with values of zero. The near-to-zero values are caused by partial X-ray penetration of the metal bars. Due to the Lambert-Beer law of attenuation

which involves taking the minus logarithm, these values will become very large compared to the rest of the data. When very high values are present in the sinogram they will dominate the reconstruction, as explained in [1]. Therefore, a threshold is used to segment the data into two parts: One part which is considered being prepresentative to the object attenuation and another part which contains the metal traces. A threshold at 0.2405 is used as a threshold and was found by visual inspection. Data below this value is replaced by zeros after the negative logarithm is taken:

$$S = \begin{cases} 0 & \text{if } -\log(T_{\text{corrected}}) > 0.24, \\ -\log(T_{\text{corrected}}) & \text{otherwise,} \end{cases} \tag{3}$$

This results in a staircasing effect with discrete boundaries in the vertical direction (detector direction) *and* in the horizontal direction (angular direction) as seen in Figure 6.

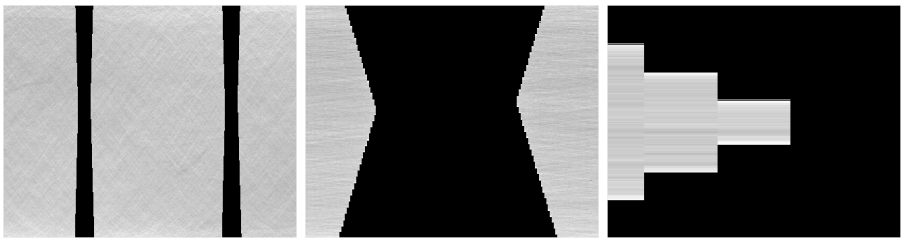

(a) *Full sinogram* (b) *Zoom* (c) *Zoom of zoom*

Figure 6: *Regular sinogram (after -log),* $S \in [0, 1.43]$*, and after values above the threshold are set to zero.*

From now, we refer to this problem as a special limited-angle (sLA) problem.

1.3 Naïve reconstruction causing streak artifacts

The built-in Matlab iradon-function is applied to the segmented sinogram to obtain the reconstruction, seen in Figure 7. A circular cut-off in the image has been used to leave out large pixel values surrounding the object, which are caused by the ROI-effect. This is done to increase the contrast in the in the image. We observe streaks with angles of about 45 and 135 degrees, but they appear somewhat more ordered than in the synchrotron reconstruction: In general, they have a specific distance between each other. The two types of streaks have same angles and we beleive they are both related to the metal bars.

The streaks are caused by the discontinuities of the truncated projections, as seen in Figure 6. These discontinuities are not inherent in the original data, but where introduced when segmenting the metal traces in the sinogram.

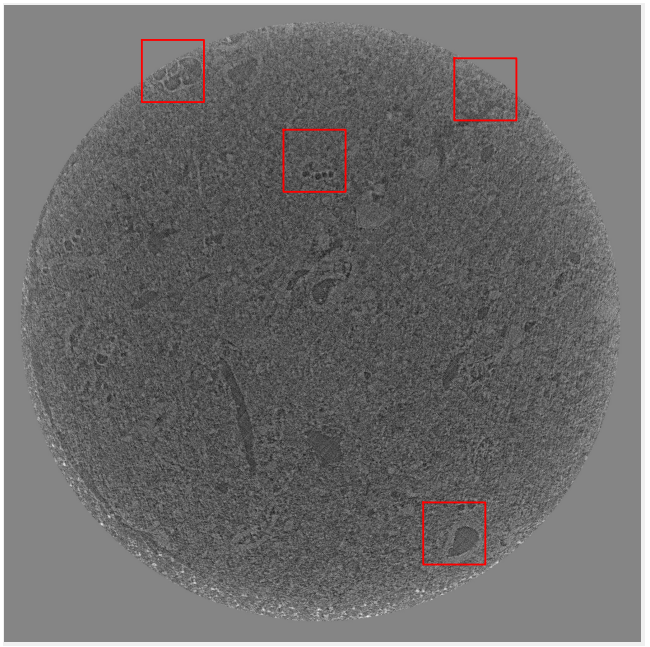

(a) *Reconstruction*

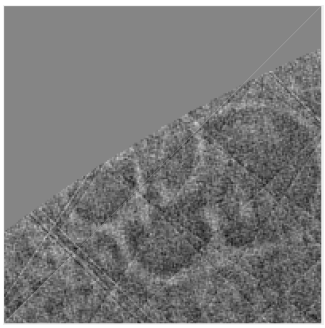

(b) *Zoom*

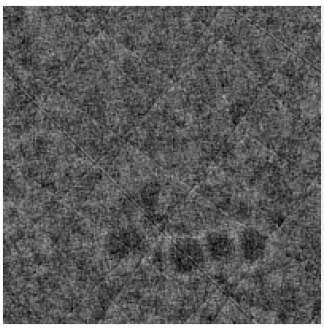

(c) *Zoom*

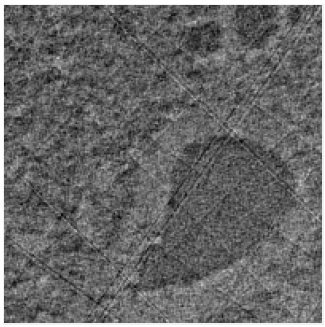

(d) *Zoom*

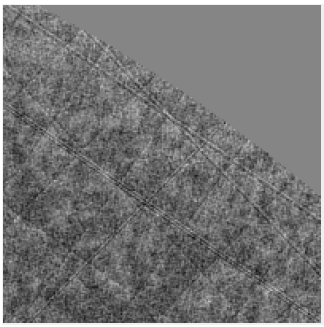

(e) *Zoom*

Figure 7: *An FBP reconstruction, based on the sinogram in Figure 6.*

1.4 Modelling the forward problem

We want to find a mask giving us the coordinates where no projections are recorded in the detectors for the angle ϕ and the radius r of the metal bars. In Figure 8 we see four metal bars, which are centered at (x, y)=(1,1), (1,-1), (-1,1), and (-1,-1). The Radon transform is the mathematical model for the data acquisition process and is expressed as follows:

$$\mathcal{R}f(\phi, p) = \int_{L(\phi,p)} f(p)dp \tag{4}$$

where L is a line described by the angle with respect to the (x,y) coordinate system, ϕ, and the distance from the origin, (x,y) = (0,0), which is denoted p:

$$L(\phi, p) = \{(x, y) \in \mathbb{R}^2 : x\cos\phi + y\sin\phi = p\} \tag{5}$$

(denotes a line with the normal direction (cos ϕ, sinϕ) and distance from the origin p.)

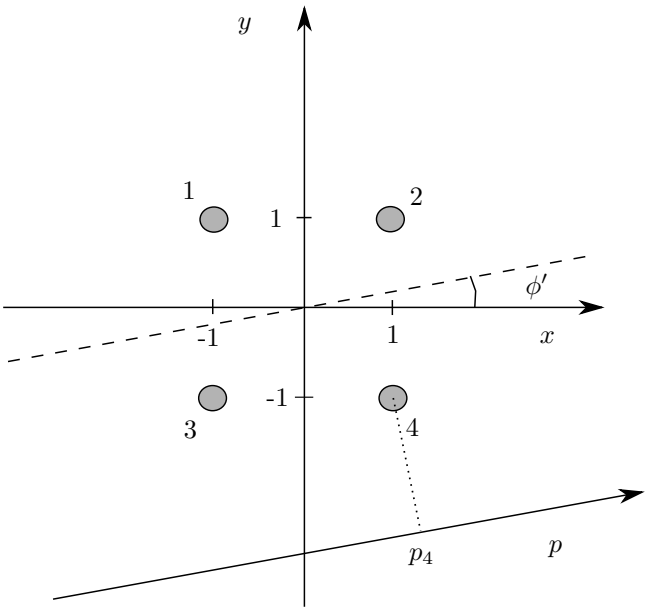

Figure 8: *The four metal bars centered at (x, y)=(1,1), (1,-1), (-1,1), and (-1,-1).*

From equation 5, we can calculate the the p-value, p_4, corresponding to the line segment, L, which passes through the fourth metal bar center at (1,-1) for angle ϕ', :

$$p_4 = 1 \cdot \cos\phi' + (-1) \cdot \sin\phi'$$

If the radius of the metal bar is r', there is no signal in the range p_{range4}

$$p_{range4} = \{p \in \mathbb{R} | \cos\phi' - \sin\phi' - r' < p < \cos\phi' - \sin\phi' + r'\}$$
$$p_{range4} = \{p \in \mathbb{R} | p_4 - r' < p < p_4 + r'\}$$

For the other metal bars the ranges are:

$$p_{range1} = \{p \in \mathbb{R} | -\cos\phi' + \sin\phi' - r' < p < -\cos\phi' + \sin\phi' + r'\}$$
$$p_{range2} = \{p \in \mathbb{R} | +\cos\phi' + \sin\phi' - r' < p < +\cos\phi' + \sin\phi' + r'\}$$
$$p_{range3} = \{p \in \mathbb{R} | -\cos\phi' - \sin\phi' - r' < p < -\cos\phi' - \sin\phi' + r'\}$$

according to the center positions of the metal bars, as depicted in Figure 9.

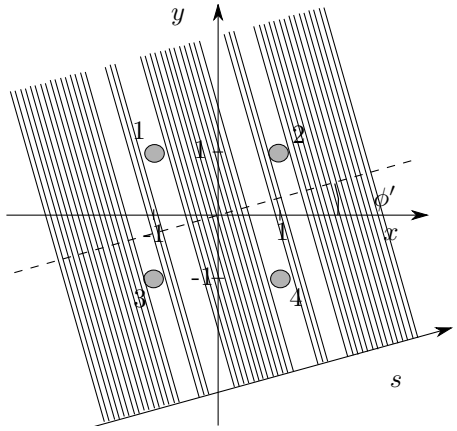

Figure 9: *For this angle, there are four ranges where projections are blocked.*

Now, we have an expression for the mask, $m(\phi, p)$:

$$m(\phi,p) = \begin{cases} 0 \quad \text{if} \left\{ p \in \mathbb{R} | \begin{cases} +\cos\phi + \sin\phi - r < p < +\cos\phi + \sin\phi + r, \\ +\cos\phi - \sin\phi - r < p < +\cos\phi - \sin\phi + r, \\ -\cos\phi + \sin\phi - r < p < -\cos\phi + \sin\phi + r, \\ -\cos\phi - \sin\phi - r < p < -\cos\phi - \sin\phi + r \end{cases} \right\}, \\ 1 \quad \text{otherwise} \end{cases} \tag{6}$$

In Figure 10a a synthesized image consisting of four metal bars and the corresponding sinogram mask are shown in 10b. At zero degrees, the left-most metal projections lie exactly on top of each other, as do the right-most metal bar projections. As the source-detector system rotates, we see all four projections, then three at 45 degrees, etc. As proceeded further to 90 degrees, the projections of the upper metal bars will lie on top of each other, as will the lower ones.

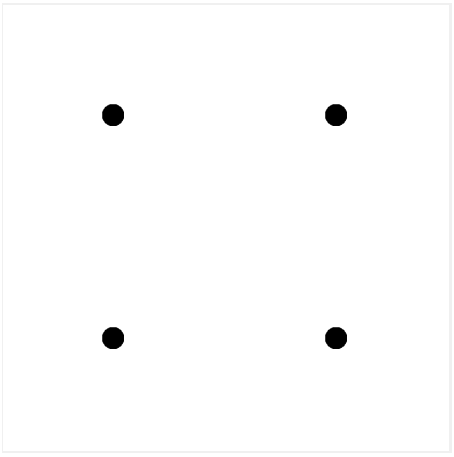

(a) *The metal bars in the object space*

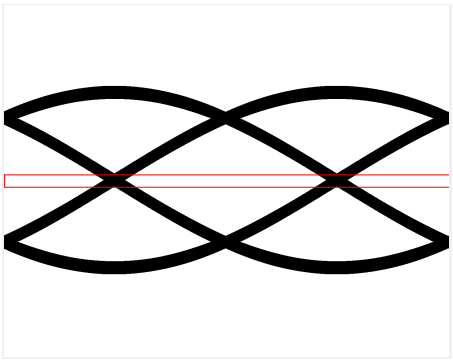

(b) *The corresponding mask in the sinogram space*

Figure 10: *An example with of an image of four metal bars and the corresponding sinogram mask.*

When the width of the detector is restricted, the limits of the sinogram ordinate (Figure 10b) changes. When the detector has the size of approximately the diameter of the metalbars in the example in Figure 10, the mask looks like the one in Figure 11. This is actually just a zoom of the full mask, indicated by the red rectangle in Figure 10b and it certainly resembles the pattern in the real data in Figure 6.

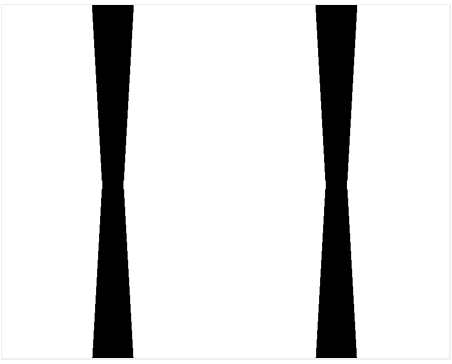

Figure 11: *This figure shows the mask, which is a zoom om the mask in Figure 10b. There are only two areas where the mask is zero and the shape of the mask resembles exactly the missing data in Figure 6.*

This mask can be used for simulating the missing data in synthetic data, as it appears in the real chalk data.

1.5 Special limited-angle in synthetic data

We want to investigate the reason for the streaks through the image in Figure 7. For this purpose, we use the Shepp-Logan phantom. The phantom and a zoom are shown in Figure 12. From this image, the corresponding sinogram can be calculated by the radon transform, and is shown in Figure 13a. For simplicity, the example is not an ROI-problem.

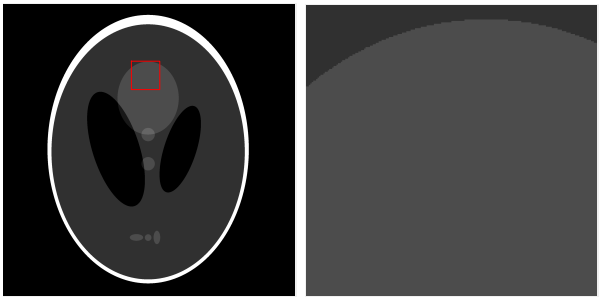

(a) *Shepp-Logan phantom* (b) *Zoom*

Figure 12: *The Shepp-Logan phantom. This will be referred to as the ground truth (GT) in Section 2.1.*

The reconstructions from the full-angle sinogram and from the sLA-sinogram (for practical reasons the mask from the data is used instead of the mask calculated in the previous section) are seen Figures 13 and 14. The full-angle reconstruction is very similar to the ground truth, although the edges are not that sharp. The sLA-reconstrucion, however, contain streaks through the image, and we can also observe some typical LA-artifacts.

(a) *Sinogram* (b) *Reconstrucion* (c) *Zoom of reconstruction*

Figure 13: *An example of a full sinogram and the correponding reconstruction. Dynamic range: [0: 1]. The reconstruction will be referred to as the full-angle reconstruction (FAR) in Section 2.1.*

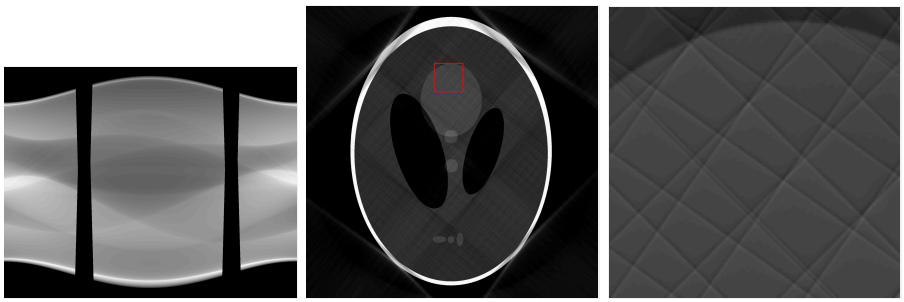

(a) *Sinogram* (b) *Reconstruction* (c) *Zoom of reconstruction*

Figure 14: *An example of a sLA sinogram and the correponding reconstruction. The dynamic range has been changed from [-.4: 1.1] to [0: 1] by truncation. The reconstruction will be referred to as the special limited-angle reconstruction (sLAR) in Section 2.1.*

These images are used to calculate quantitative measures of the image qualities. This will be done in Section 2.1.

2 Description of artifacts

2.1 Quantification

Section 3 investigates a number methods to reduce the artifacts in the reconstructions. To compare these methods, a range of objective image quality measurements are chosen to quantify reconstruction quality before and after applying the artifact reduction methods. As a beginning, we only deal with the quantification of artifacts before applying the artifact reduction methods.

2.1.1 Quantification methods for real and synthetic data

The measures require a reference image and a distorted image. Normally, the reference image is a ground truth, and the distorted image is then a reconstruction. For the real data case we do not have a ground truth available, but in the synthetic data case, we do have a ground truth. Therefore, we treat the artifact quantification differently:

Synthetic data As synthetic data, we will use the Shepp-Logan phantom, as shown in Figures 12, 13b, and 14b. In the case of synthetic data, the reference images are the ground truth (GT), (Figure 12) or the full-angle reconstrucion (in Figure 13b and the distorted images are the special limited-angle reconstruction (sLAR), (Figure 14b) or the full-angle reconstrucion (in Figure 13b. This makes it possible to relate measures across synthetic and real reconstructions and also to relate GT/FAR and GT/sLAR, and we expect the GT/sLAR difference to be larger than the GT/FAR difference.

Real data We have a full data set of chalk available resembling the data we are working with in this report. This data set will be referred to as ERDA-data. The full-angle sinogram and the corresponding FBP reconstructions are shown in Figure 15. The reconstruction from this data is used as the reference image, even though it is not the ground truth. Applying the sLA-mask on the sinogram and reconstructing from this, gives an image which is used as the distorted image. The sLA-sinogram and corresponding reconstruction are shown in Figure 16.

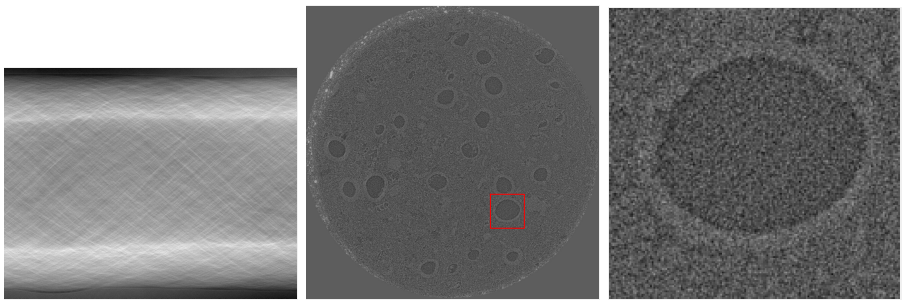

(a) *Sinogram* (b) *Reconstruction* (c) *Zoom of reconstruction*

Figure 15: *Full-angle ERDA sinogram and the corresponding FBP-reconstruction. This reconstruction (ERDA FAR) will be used as the reference image when comparing the image quality with the ERDA sLAR in figure 16b.*

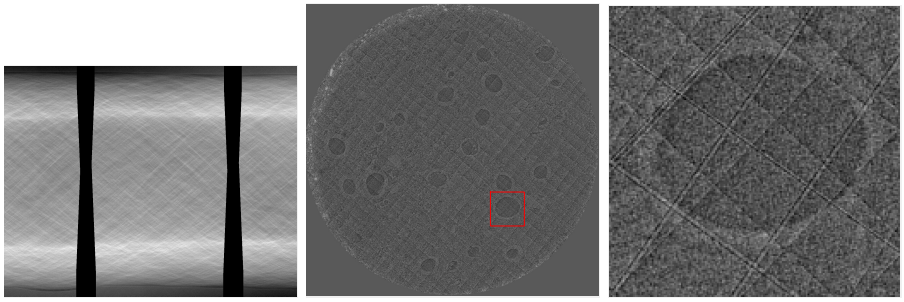

(a) *Sinogram* (b) *Reconstruction* (c) *Zoom of reconstruction*

Figure 16: *Special limited-angle ERDA sinogram and the corresponding FBP-reconstruction. This reconstruction (ERDA sLAR) will be used as the distorted image when comparing the image quality with the ERDA FAR in figure 15b.*

The numbers produced for synthetic and real data cases, will be compared with the numbers *after* the artifact reducing methods are applied.

The chosen measures Following measures are chosen:

1. The root-mean-square error (RMSE):

$$\mathrm{RMSE} = \left(\frac{1}{NM} \sum_{i=1}^{M} \sum_{j=1}^{N} |R(i,j) - D(i,j)|^2 \right)^{\frac{1}{2}},$$

where N and M are number of rows and colums, respectively in the images R and D, representing the reference image and the distorted image, respectively. This measure is a standard measure, used for pixelwise comparison in images.

2. Histogram Similarity Measure (HSM) :

$$\text{HSM} = \left(\frac{1}{2NM} \sum_i |h_R(i) - h_D(i)|^2 \right)^{\frac{1}{2}},$$

h_R and h_D the histograms of the reference image and distorted images, respectively, and i runs over all elements in the histograms. The two histograms have same number of bins running from the lowest pixel value, $\min(R, D)$, to the largest pixel value, $\max(R, D)$, of the two images. The streaks in the distorted image consist of dark lines, each with a light "shade" next to it. Therefore, the two histograms will probably look different: The histogram for the distorted image may contain peaks/larger peaks at specific pixel values than the reference image. This measure is related to - and inspired by - the measure Ordered Histogram Similarity Measure, found in [3].

3. Spectral Magnitude Distortion (SMD) [3]:

$$\text{SMD} = \frac{1}{MN} \sum_{i=1}^{M} \sum_{j=1}^{N} |M_R(i,j) - M_D(i,j)|^2,$$

where M_R and M_D are the power spectra of the reference image and the distorted image, respectively. Since the streaks appear with a distance that look rather constant, this will show as a peak in the distorted power spectrum. Both elements of high frequency (representing the single streaks) and low frequencies (representing the spacing between the parallel streaks) will appear. Therefore, this measure is also included in the benchmarking.

We expect all values of the quality measures to be smaller for similar images than for different images because they indicate some kind of distance between the images.

2.1.2 Reporting the values of the measures

Synthetic data We are comparing two types of images: One comparison between the ground truth (GT) and the full-angle reconstruction (FAR), and another comparison between the GT and the sLA reconstruction (sLAR). This is done for the images shown in Figures 12, 13, and 14. We expect that GT and FAR images look more alike than the GT and sLAR images do, because sLAR contain streak artifacts. Therefore, we expect that all measures are higher for the GT/sLAR comparison than for the GT/FAR comparison is. In table 1 the results are shown. The relation between the values are in correspondence with our expectations.

Shepp-Logan	RMSE	HSM	SMD	MI
GT/FAR	0.0295	0.2559	36.25	1.394
GT/sLAR	0.0678	0.3332	42.85	1.284
FAR/sLAR	**0.0606**	**0.1549**	**9.442**	1.621

Table 1: *Image quality measurements for the synthetic data. The measurements in the lowest row will be compared with same measurements after applying the artifact reduction methods (not the MI).*

Real data For the real data, we do not have access to a ground truth. Therefore, the full-angle reconstruction (ERDA-FAR) is compared with the special limited-angle reconstruction (ERDA-sLAR). The measures are shown in table 2.

ERDA	RMSE	HSM	SMD	MI
FAR/sLAR	**1.17e-4**	**0.0012**	**0.0311**	1.04

Table 2: *Image quality measurements for the real data. The measurements will be compared to the same type of measurements after applying the artifact reduction methods.*

2.2 Where and why do the artifacts occur?

To illuminate the position of the streaks, two masks are applied to the Shepp-Logan phantom sinogram: A pure limited-angle (LA) mask and one type of a special limited-angle (sLA) mask in Figure 17a and 17b, respectively. The pure LA sinogram contains edges in the angular direction, whereas the sLA sinogram contains edges in the angular direction *as well as* in the detector direction, p, as the SPring-8 data does. The detector-directed edges are a consequence of the extra "tip" being present. The difference of the two sinograms is shown in Figure 17c. The FBP-reconstructions of the LA, the sLA, and the difference sinograms are shown Figure 17d, 17e, and 17f, respectively. The reconstruction from the difference sinogram can also be obtained by subtracting the LA reconstruction from the sLA reconstruction, since FBP is a linear operation with respect to the angles.

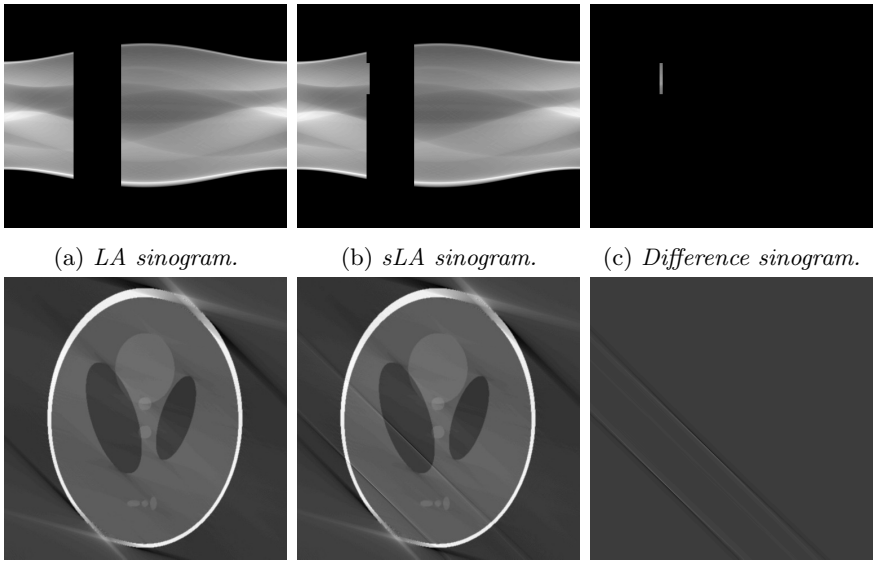

(a) *LA sinogram.* (b) *sLA sinogram.* (c) *Difference sinogram.*

(d) *Reconstruction from LA sinogram.* (e) *Reconstruction from LA sinogram with tip.* (f) *Reconstruction from difference sinogram.*

Figure 17: *Illustration of the effect of one small tip.*

The micro-local analysis ([5]) describes streak artifacts in LA-reconstructions as are viewed in Figure 17d; Their intensity scale with the edge intensities in the reconstruction and only emerge from edges in the reconstruction. Further, they have an angle perpendicular to the cut-off angles in the sinogram. As a convention, singularities (edges) are described by the tuple, (x, ξ) in image space, where x is the singular position in $\mathbb{R}^2$ and ξ is the singular direction (normal to the edge). For parallel-beam tomographic problems, one can only expect to reconstruct edges (x, ξ), where ξ is in the angular range of the data space, Φ. For the pure LA-example in Figure 17, $\Phi = \{\phi \in \mathbb{R} \mid 0° \leq \phi \leq \phi_1, \phi_2 \leq \phi < 180°\}$, where $\phi_1 = 45°$ and $\phi_2 = 75°$ are the LA cut-off angles. This means that edges in the image domain with angles in the interval $\phi_1 \leq \Xi_{missing} \leq \phi_2$ are not reconstructed, as can be observed in the reconstruction in Figure 17d.

The reconstruction based on the sLA sinogram in Figure 17e contains additional artifacts on top of the typical LA artifact. The artifacts consist of two parallel streaks positioned in the lower left part of the reconstruction, which clearly stand out in the difference reconstruction in Figure 17f. Keep in mind that: 1) each point in a sinogram corresponds to a line in the reconstruction with a specific angle and projection displacement, p, and 2) backprojections start at $\phi = 0$, which is vertically directed. The angular position of the "tip" in the sinogram, $\phi_1 + \epsilon$, where ϵ is a very little andular displacement, corresponds to the angle of the two streaks in the reconstruction. Also, they are separated by a distance corresponding to the distance between the vertical cut-offs in the

difference sinogram. Actually, the position and angle of the upper streak in the reconstruction correponds exactly to the position of lower edge of the tip in the sinogram. Likewise, the position and angle of the lower streak correponds exactly to the position of upper edge of the tip.

If the angular width of the "tip" is increased, four streaks through the reconstruction appears and an area being overexposed, as seen in the example in Figure 18e and 18f. Here, the positions and angles of the four streaks correpond exactly to the positions of the corners of the square-shaped data in the difference sinogram.

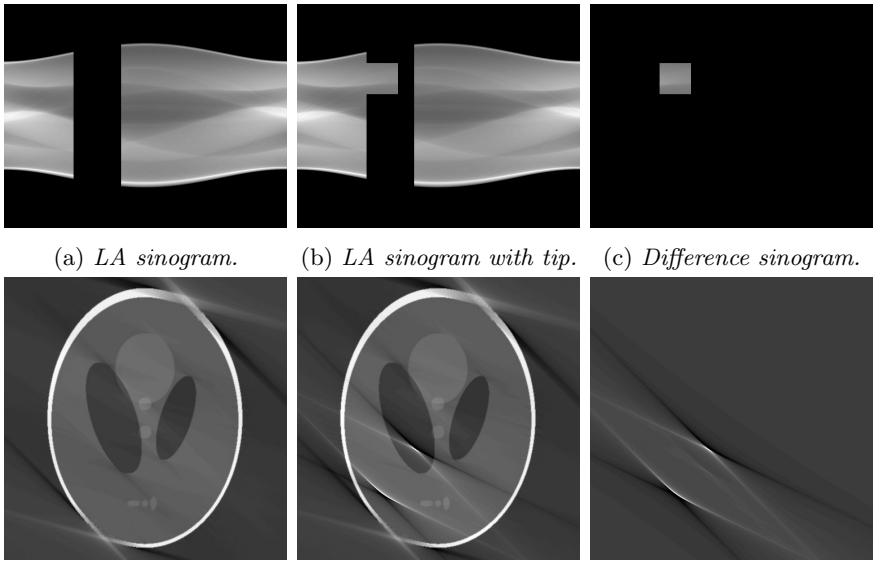

(a) *LA sinogram.* (b) *LA sinogram with tip.* (c) *Difference sinogram.*

(d) *Reconstruction from LA sinogram.* (e) *Reconstruction from LA sinogram with tip.* (f) *Reconstruction from difference sinogram.*

Figure 18: *Illustration of the effect of a large tip.*

Nearby the intersections of the streaks, the streaks appear stronger than further away from the intersections where they are more blurry. Further, at the intersections each streak flips the intensity from dark to light or from light to dark. The overexposure can be explained by help of the difference sinogram and corresponding reconstruction, in Figure 18c and 18f: Since the backprojected data only covers a certain area of the image, this additional data adds to a higher pixel value in this specific area than in the rest of the image.

Adding extra data, as has been done in the example in figure 18b compared to the example in Figure 17b, also adds more information, which then gives a better reconstruction. Figure 19a and 19b show zooms of the left oval of the LA reconstruction and the sLA reconstructions from Figure 18, respectively. In the sLA reconstruction, the edge of the oval is closed whereas the oval is not

closed and smeared out for the LA reconstruction. For better comparison, these zooms have higher resolution than the other reconstructions.

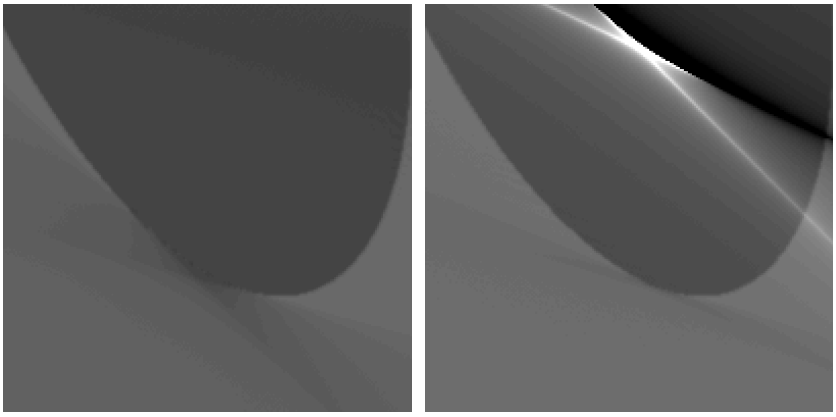

(a) *LA reconstruction. Edges in* $\phi_1 \leq \Xi_{missing} \leq \phi_2$ *are not reconstructed.*

(b) *Reconstruction from LA sinogram with large tip. Edges in* $\phi_1 + \delta \leq \Xi_{missing} \leq \phi_2$ *are not reconstructed, where* δ *is the width of the tip in figure 18b.*

Figure 19: *Zooms of Figure 18d and 18e, showing that more data provides better reconstructions*

The tip in the sinogram covers the left oval in the Shepp-Logan phantom in the backprojection, providing a better edge reconstruction in this specific area. Therefore, the translational and angular position of the tip determine which area of the image to be reconstructed better than if the tip were not there. The angular position of the tip determines which edge angles are reconstucted better than if the tip were not there.

In figure 20, it is illustrated how the number of sLA-induced streaks in the reconstruction reflects the number of steps in the sinogram; There is exactly one streak for each non-smooth edge in the sinogram. Since each step provides two non-smooth edges in the sinogram this results in two streaks in the reconstruction per step. The streaks caused by the limited-angle are still present but are not as pronounced, though. This is because those density jumps are not as pronounced as they are for the non-smooth edges of the tips.

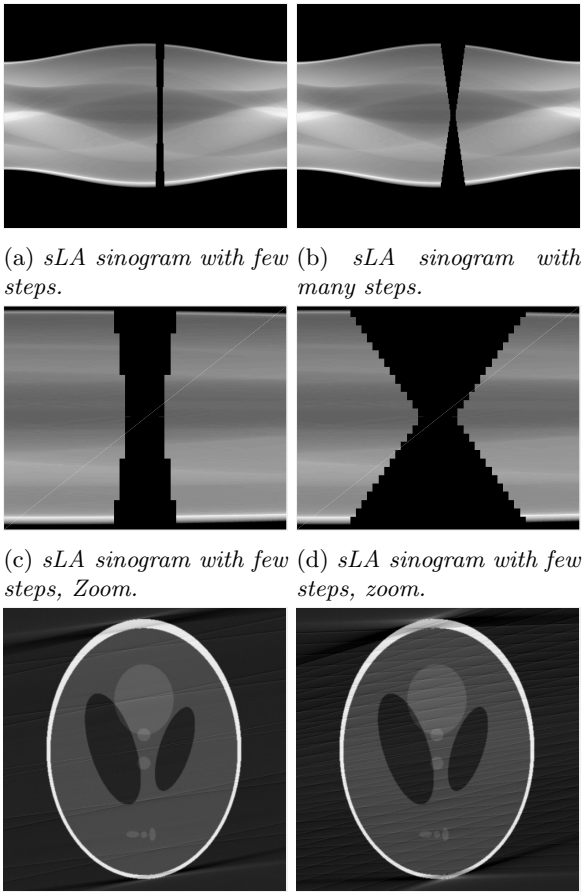

(a) *sLA sinogram with few steps.*

(b) *sLA sinogram with many steps.*

(c) *sLA sinogram with few steps, Zoom.*

(d) *sLA sinogram with few steps, zoom.*

(e) *Reconstruction, few streaks.*

(f) *Reconstruction, many streaks.*

Figure 20: *Illustration of the effect of the number of steps. There is exactly one streak for each non-smooth edge (corner) in the sinogram.*

Figure 21 illustrates how the angular position of the missing data in the sLA sinogram affects the angle of the streaks in the reconstruction. When the missing data has an angle $\phi \simeq 45°$, the streaks in the reconstruction have correspondedly the angle $\xi \simeq 45°$, as observed in Figure 21a and 21c. Likewise, when the missing data is shifted to $\phi \simeq 100°$ the streaks in the reconstruction have the angle $/xi \simeq 100°$, as viewed in Figure 21b and 21d.

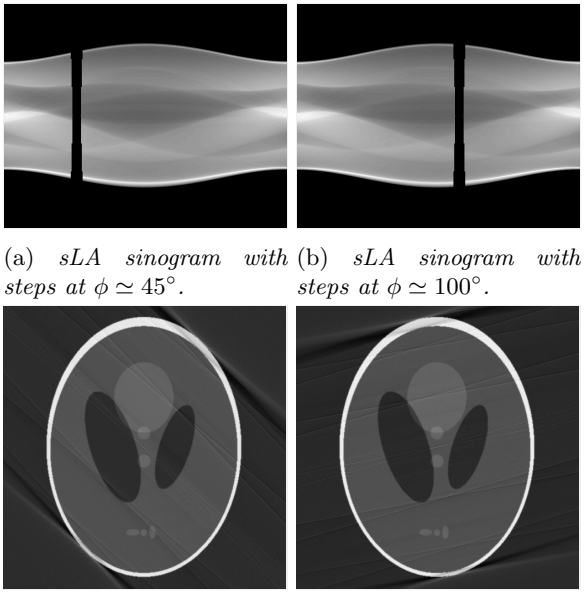

(a) *sLA sinogram with steps at* $\phi \simeq 45°$.

(b) *sLA sinogram with steps at* $\phi \simeq 100°$.

(c) *Streaks in corresponding reconstruction have slope* $\xi \simeq 45°$.

(d) *Streaks in corresponding reconstruction have slope* $\xi \simeq 100°$.

Figure 21: *This figure illustrates how the angular position of the steps in the sLA sinogram translates directly to the slope of the streaks in the corresponding reconstruction.*

In conclusion, this section argues that the streaks in the reconstruction appear when edges are present in the sinogram.

3 Artifact reduction methods

As discussed in Section 2, the boundary of the missing data gives rise to streaks in the image. This means that if we get rid of the singularities at the boundary, we also get rid of the streaks. Following two methods suggest ways of doing that.

3.1 Setting truncated projections to zero

If the truncated projections are all set to zero, then we are left with a pure LA-problem. Although artifacts do occur in this case, they are typically not as pronounced because the streak intensity scales with singularities in the data at the boundary (as described in [5]).

In Figure 22 this method is illustrated on the Shepp-Logan phantom for a sinogram with one big tip.

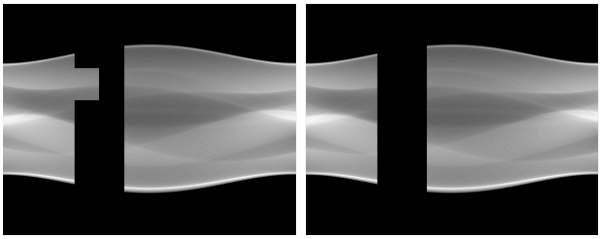

(a) *sLA sinograms and reconstrucions.*

(b) *sLA sinograms and reconstrucions.*

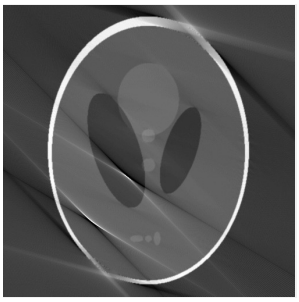

(c) *sLA sinograms and reconstrucions.*

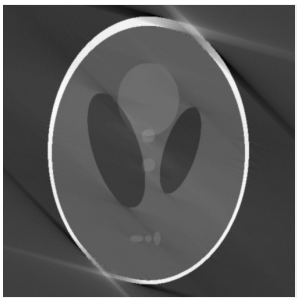

(d) *sLA sinograms and reconstrucions.*

Figure 22: *sLA sinograms and reconstrucions.*

Figures 23a and 23c show the sinogram and its zoom when the data mask is applied. Figures 23b and 23d show the sinogram and its zoom after removing the truncated projections, constructing a LA-problem.

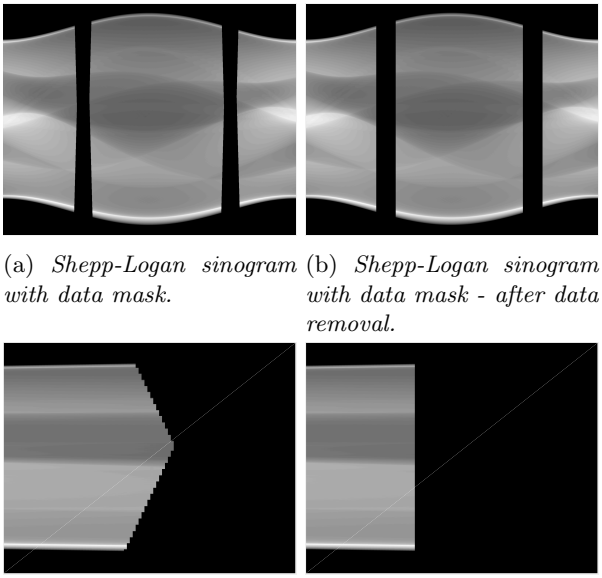

(a) *Shepp-Logan sinogram with data mask.*

(b) *Shepp-Logan sinogram with data mask - after data removal.*

(c) *Shepp-Logan sinogram with data mask, zoom.*

(d) *Shepp-Logan sinogram with data mask - after data removal, zoom.*

Figure 23: *sLA sinograms and reconstrucions.*

Figure 24 shows the reconstructions before and after removal of truncated projections in the sinogram, together with their zooms.

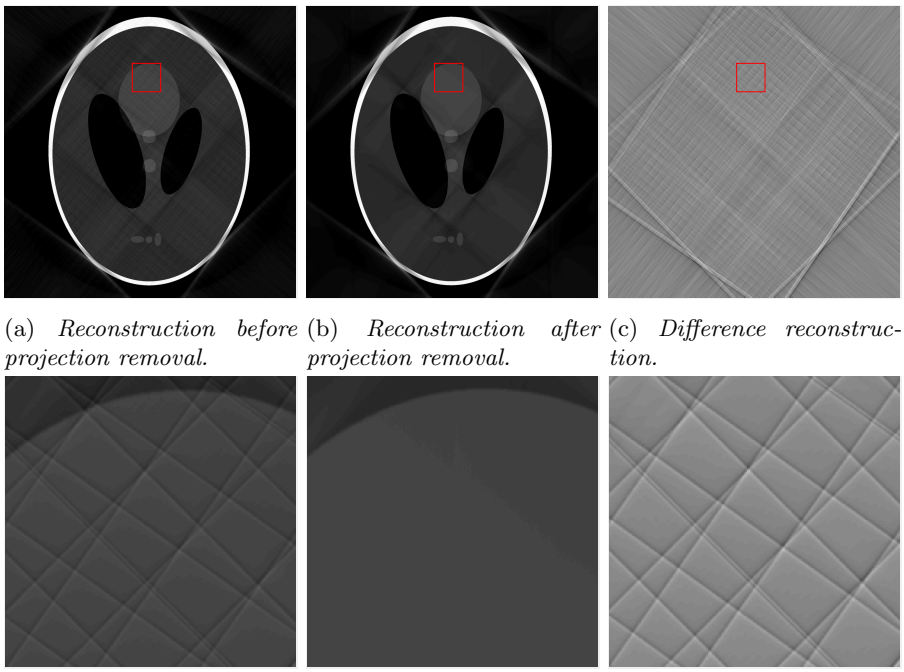

(a) *Reconstruction before projection removal.* (b) *Reconstruction after projection removal.* (c) *Difference reconstruction.*

(d) *Reconstruction before projection removal - zoom.* (e) *Reconstruction after projection removal - zoom.* (f) *Difference reconstruction - zoom.*

Figure 24: *LA reconstrucions based on the databased mask.*

The method clearly removes the artefacts for synthetic data.

3.2 Damping truncated projection

Regional smoothing can be obtained by multiplying the sinogram with a function that dampens the projections across edges. The edges can be either in the detector direction or in the angular direction. Likewise, we can make functions that smoothes the projection edges in either the detector direction or the angular direction. The function goes from zero to one and this transition can be varied and include an arbitrary number of pixels.

Damping projections across edges in angular direction Figures 25 and 26 shows that smoothing the edges in the angular direction only decreases the LA-artifacts. The angular-directed edge smoothing does not remove the bright/dark streaks completely. The problem may be viewed as a variant of a region-of-interest (ROI) problem in which the size of the region of interest has the size of the truncated projections. In typical ROI-problems, the ROI covers all 180 degrees and a bright artifact surrounds the illuminated region. If the present data only consisted of the truncated projections covering 180 degrees, a bright circle would surround the ROI. Here, the truncated projections only

cover approx. 20 degrees, and therefore only 2×20 degrees $= 40$ degrees of the circular artifact is present in the reconstruction as described in Case II, ii), b). There is some smoothing of the streaks farther away from the center of the region of interest (ROI). One explanation could be that every single truncated projection balance other truncated projections, and the last ones are dampened in a smooth way by the smoothing function. This method, however, does not account for the ROI-effects, and therefore does not remove the small circular effects near the ROI.

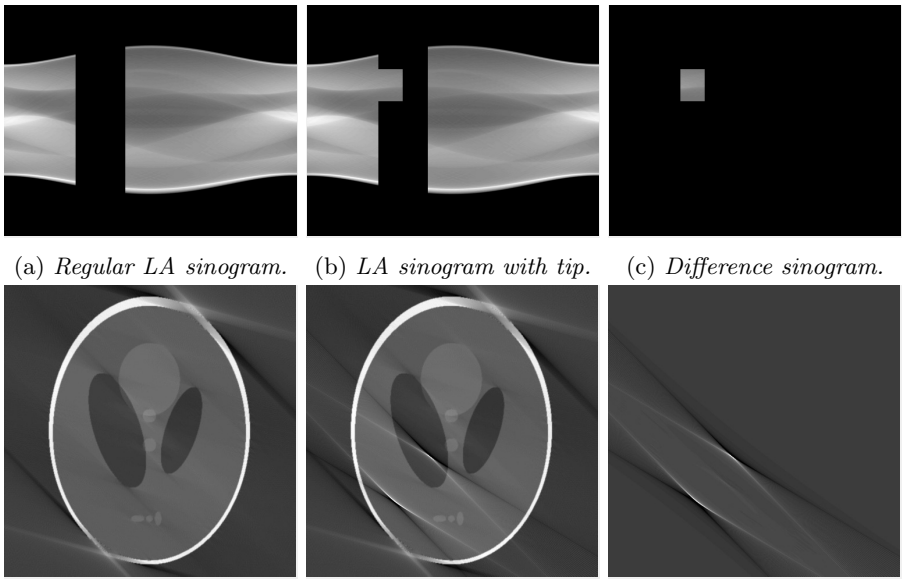

(a) *Regular LA sinogram.* (b) *LA sinogram with tip.* (c) *Difference sinogram.*

(d) *Reconstruction of LA sinogram.* (e) *Reconstruction of LA sinogram with tip.* (f) *Difference reconstruction.*

Figure 25: *sLA sinograms and reconstrucions.*

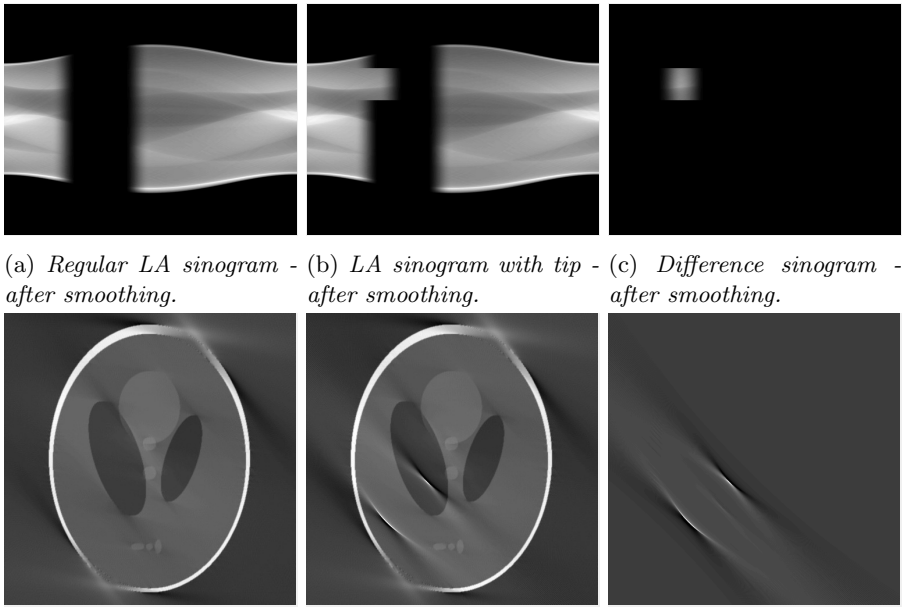

(a) *Regular LA sinogram - after smoothing.*

(b) *LA sinogram with tip - after smoothing.*

(c) *Difference sinogram - after smoothing.*

(d) *Reconstruction from regular LA sinogram after smoothing.*

(e) *Reconstruction from LA sinogram with tip after smoothing.*

(f) *Difference reconstruction - after smoothing was performed.*

Figure 26: *Smoothing in angular direction*

Damping projections across edges in detector direction When smoothing the truncated projection boundaries in the detector direction, the streaks are reduced, as seen in Figure 27. However, an overexposure is present due to the extra data being backprojected.

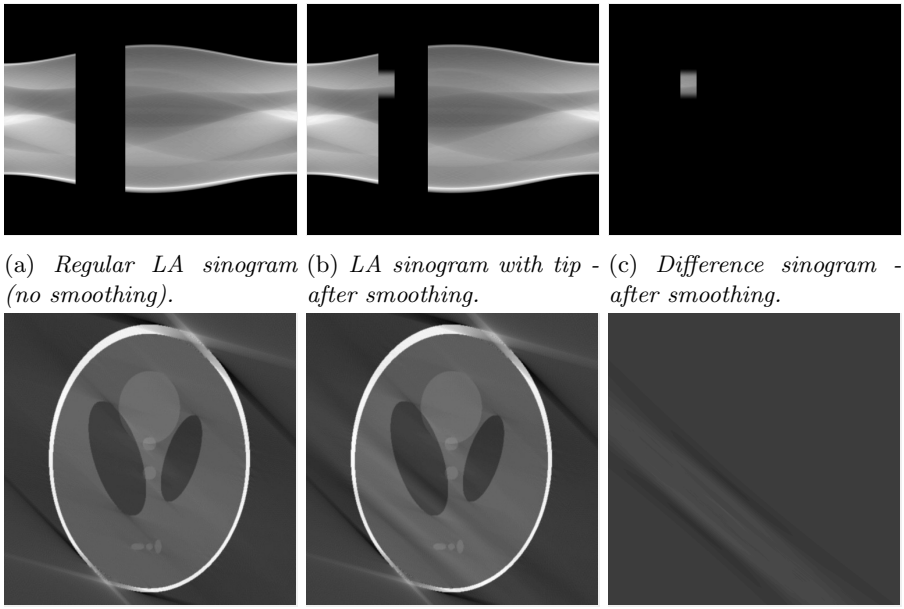

(a) *Regular LA sinogram (no smoothing).* (b) *LA sinogram with tip - after smoothing.* (c) *Difference sinogram - after smoothing.*

(d) *Reconstruction from regular LA sinogram after smoothing.* (e) *Reconstruction from LA sinogram with tip after smoothing.* (f) *Difference reconstruction - after smoothing was performed.*

Figure 27: *Smoothing in detector direction.*

In Figure 28 the effect of detector-directed smoothing for the Shepp-Logan image with databased mask is illustrated. As a result, the streaks are greatly dampened. However, shades are present in the reconstruction, seen in Figure 28e. These shades were removed when the truncated projections are removed in the LA-case in Figure 28. Increasing the smoothing transition from 40 to 60 pixels greatly reduces the effect of the shades (the reconstruction is 2048 $\times$ 2048).

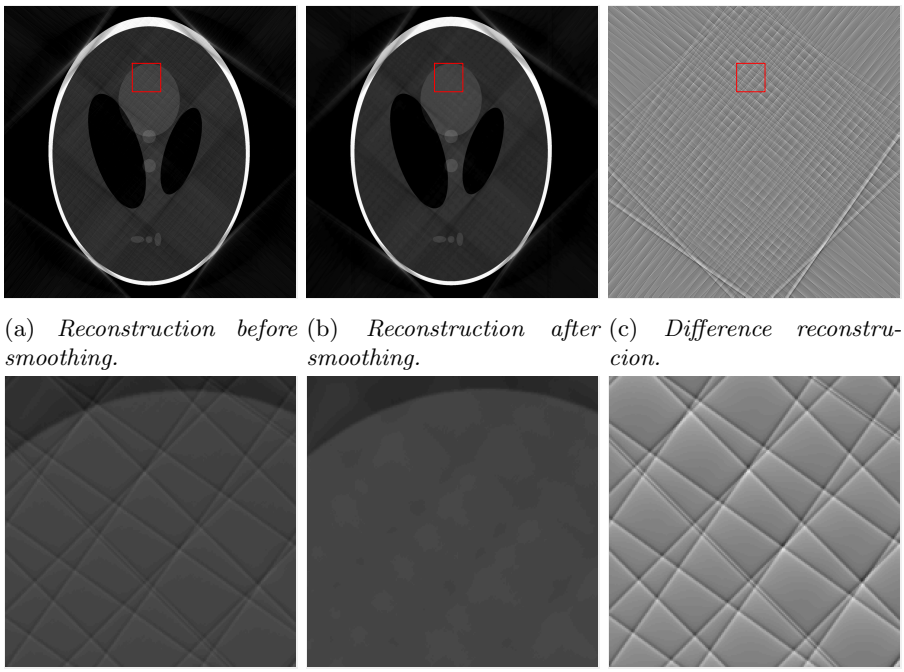

(a) *Reconstruction before smoothing.* (b) *Reconstruction after smoothing.* (c) *Difference reconstrucion.*

(d) *Reconstruction before smoothing - zoom.* (e) *Reconstruction after smoothing - zoom.* (f) *Difference reconstruction - zoom*

Figure 28: *sLA sinograms and reconstrucions.*

4 Results

4.1 Setting truncated projections to zero

Remember that the truncated projections are the projections where the effective width of the detector is decreased. When these projections are set to zero, the non-smooth edges in the sinogram are also removed, and the problem turns into a regular LA-problem. Although artifacts do occur in this case, they are typically not as pronounced as when the edges are detector-directed because the streak intensity depends on the intensity differences in the image at $\mathrm{bd}(A)$. Real data always contains noise. Tomographic noise is Poission distributed but for a high number of photons, which is almost always the case, the distribution approximates to a Gaussian distribution. This means that sharp edges become less sharp in an image, which then means that streak artifacts caused by angular-directed edges are even less pronounced. In Figure 29a and 29c the original sinogram after -log and thresholding has been performed on the transmission sinogram is shown together with its zoom. To the right the result of setting the truncated projections in the sinogram to zero is shown together with its zoom in Figure 29b and 29d, respectively.

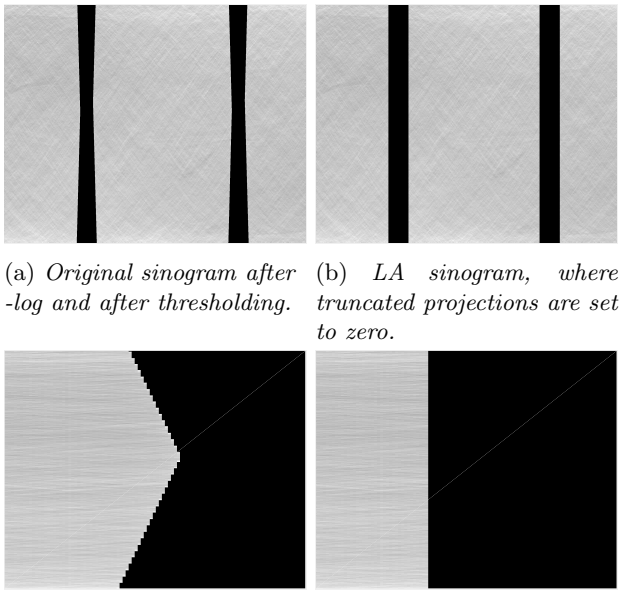

(a) *Original sinogram after -log and after thresholding.*

(b) *LA sinogram, where truncated projections are set to zero.*

(c) *Original sinogram after -log and after thresholding, zoom.*

(d) *LA sinogram, where truncated projections are set to zero, zoom.*

Figure 29: *Comparison between original and LA sinograms, where truncated projections are set to zero.*

The reconstructions of the original sinogram and LA-sinogram together with

their difference are shown in Figure 30.

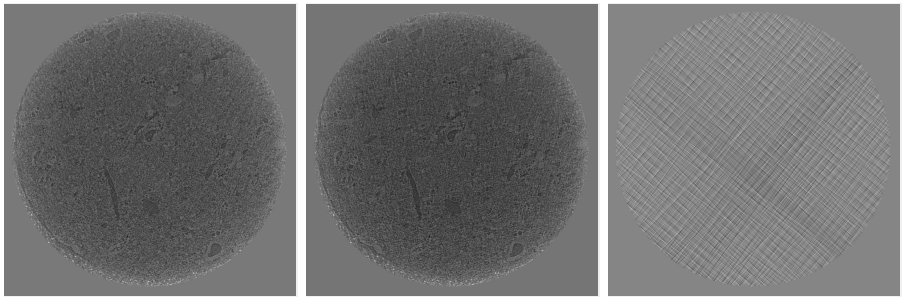

(a) *Reconstruction of the original sinogram.* (b) *Reconstruction of the LA sinogram.* (c) *Difference between the reconstructions.*

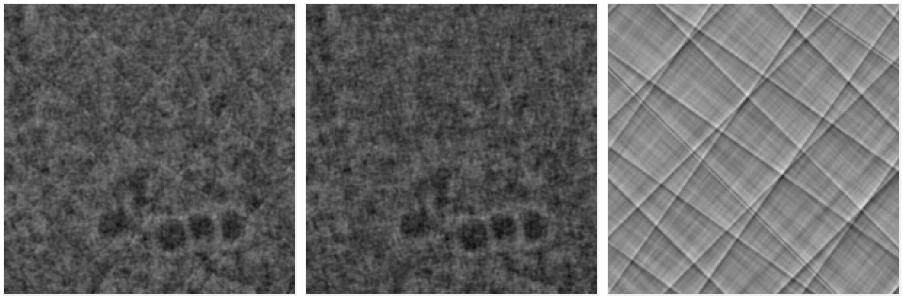

(d) *Reconstruction of the original sinogram, zoom.* (e) *Reconstruction of the LA sinogram, zoom.* (f) *Difference between the reconstructions, zoom.*

Figure 30: *Reconstructions of the original sinogram and the LA sinogram and their zooms.*

Figure 30a and 30d show the reconstruction from the original sinogram and its zoom, respectively, where streaks are present. Figure 30b and 30e show the reconstruction from the LA sinogram and its zoom, respectively, where streaks are not present any longer. At last Figure 30c and 30f show the difference of the two types of reconstructions and its zoom, respectively, which show pronounced streaks plus some underlying structure. The two last figures illustrate that the streaks are removed from the reconstruction when reconstructing from the LA sinogram. However, the underlying structure suggests that additional information is removed due to "removal" of the projections.

Removal of data - as is done in this case - causes a decrease in reconstruction quality. As discussed in Section 2.2 and illustrated in Figure 19 it may even lead to loss of edge information in specific areas of the image for edges with angles corresponding to the angular position of the missing data. This may be a problem because the edges in particular are important in image segmententation. In this specific situation only a small portion of the sinogram is set to zero. For problems where the truncated projections span a larger angular range, the consequence of removing all truncated projections would be more severe. This

would lead to greater loss of data, hence a worse reconstruction and less edge information. Therefore, another method is investigated.

4.2 Smoothing truncated projections in the detector direction

This method operates near the bd(A) only, which minimizes the loss of data. As was discussed earlier the non-smooth bd(A) causes streaks. In this method we smooth bd(A) in the detector direction, only. By doing this we remove artifacts. This time, however, we still have the information from the tips. In Figure 31 the original sinogram and the detector smoothed sinogram and their zooms are shown.

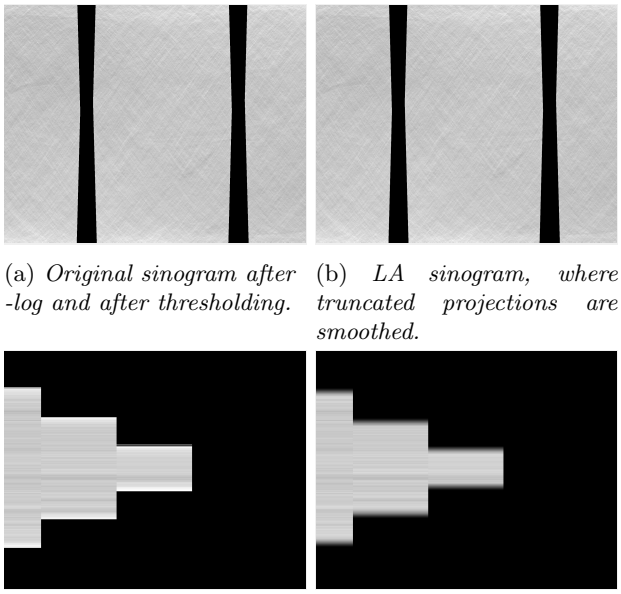

(a) *Original sinogram after -log and after thresholding.*

(b) *LA sinogram, where truncated projections are smoothed.*

(c) *Original sinogram after -log and after thresholding, zoom.*

(d) *LA sinogram, where truncated projections are smoothed, zoom.*

Figure 31: *Comparison between original and detector smoothed sinograms.*

The reconstructions corresponding to the sinograms in Figure 31 together whith their difference are shown in Figure 29. The shadows that we saw in the simulated Shepp-Logan data are not visible in these reconstructions. This is probably due to the greater variance and noise in the chalk data. It is, however, very likely that the shadows are still there, but not visible to the naked eye.

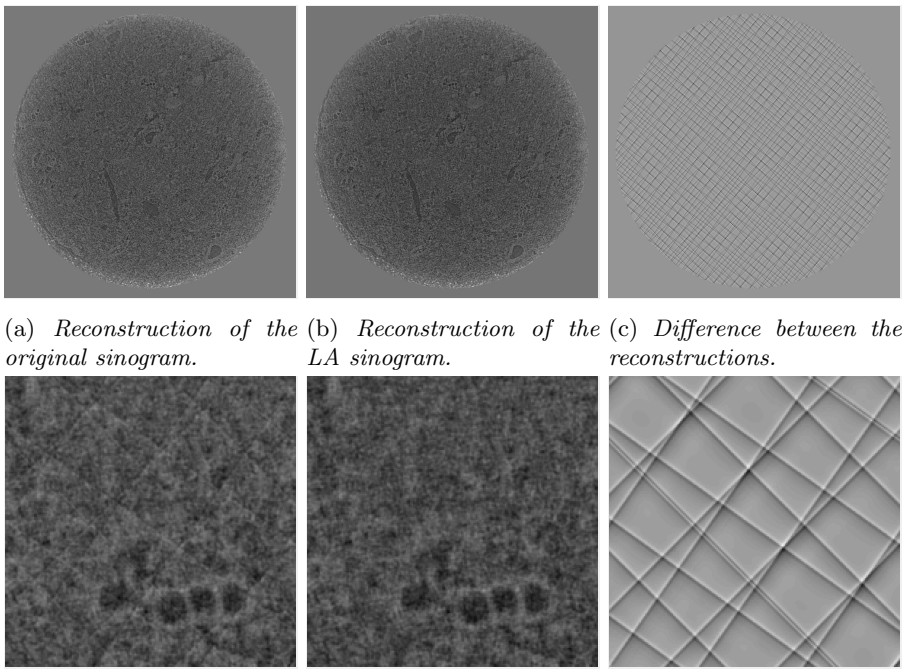

(a) *Reconstruction of the original sinogram.* (b) *Reconstruction of the LA sinogram.* (c) *Difference between the reconstructions.*

(d) *Reconstruction of the original sinogram, zoom.* (e) *Reconstruction of the LA sinogram, zoom.* (f) *Difference between the reconstructions, zoom.*

Figure 32: *Reconstructions of the original sinogram and the LA sinogram and their zooms.*

This time the background of the reconstruction difference close to zero as opposed to the reconstruction difference in Figure 30. This indicates that less information is lost when smoothing than when setting the truncated projections to zero.

4.3 Quantification of improvements

4.3.1 Synthetic data comparison

The measures from before the methods were applied are shown in (Table 3). The numbers in the following tables are almost all consistent. For simplicity, it is possible to focus on one measure, the SMD, for instance, which is highlighted.

Shepp-Logan	RMSE	HSM	SMD	MI
GT/FAR	0.0412	0.2537	52.95	1.379
GT/sLAR	0.0730	0.3331	57.2107	1.269
FAR/sLAR	0.0606	0.1352	**9.44**	1.636

Table 3: *Synthetic data - before applying methods.*

After the methods were applied, a comparison between the full-angle reconstruction (FAR) and the two methods are shown in Table 4.

Shepp-Logan	RMSE	HSM	SMD
FAR/Method LA	0.0644	0.1375	**6.5074**
FAR/Method smooth	0.0603	0.1359	**6.3167**

Table 4: *Synthetic data - after applying methods. Compare with full-angle reconstruction (FAR).*

When comparing the two tables, the numbers in Table 3 for FAR/sLAR are all larger than they are for the corresponding measures in Table 4. This indicates that after applying either of the methods, the image quality improved. It can also be noted that the measures for smoothing the edges are all smaller than the measures for converting the sinogram into an LA-problem. This indicates that smoothing the edges results in better reconstructions than when converting the sinograms into LA-problems.

Also, a comparison between the special limited-angle reconstruction (sLAR) and the two methods are shown in Table 5. These measures are calculated to compare the two methods. As in Table 4 all measure indicate that smoothing is better than converting into LA since all numbers are smaller for smoothing than for LA.

Shepp-Logan	RMSE	HSM	SMD
sLAR/Method LA	0.0170	0.0130	**5.4467**
sLAR/Method smooth	0.0146	0.0096	**5.1289**

Table 5: *Synthetic data - after applying methods. Compare with special limited-angle reconstruction (sLAR).*

4.3.2 Full data set (small area of image) comparison

The smoothing transition consists of 60 pixels. When comparing the methods in real data, the measures indicate exactly the same as for the Shepp-Logan phantom. Firstly, all measures are larger in Table 6 than in Table 7 exept one measure, indicating that applying the methods is better than doing nothing.

In Table 6 the comparison between FAR and sLAR is performed.

ERDA	RMSE	HSM	SMD
FAR/sLAR	1.1217e-04	6.0990e-05	**2.8698e-04**

Table 6: *Real data - before applying methods.*

Secondly, when comparing the numbers in first and second row of Table 7 the numbers are all smaller for the smoothing method than for the LA method, indicating that smoothing provides a better reconstruction than converting to LA.

ERDA	RMSE	HSM	SMD
FAR/Method LA	7.7210e-05	9.8002e-05	**2.0714e-04**
FAR/Method smooth	5.8624e-05	5.3344e-05	**1.5417e-04**

Table 7: *Real data - after applying methods. Compare with full-angle reconstruction (FAR).*

Again, when comparing the numbers in first and second row of Table 8 the numbers are all smaller for the smoothing method than for the LA method, consolidating that smoothing provides a better reconstruction than converting to LA.

ERDA	RMSE	HSM	SMD
sLAR/Method LA	1.1487e-04	1.2578e-04	**2.5911e-04**
sLAR/Method smooth	9.8318e-05	7.1078e-05	**2.2142e-04**

Table 8: *Real data - after applying methods. Compare with special limited-angle reconstruction (sLAR).*

4.3.3 P-cubed data (small area of image) comparison

The measures found when comparing sLAR with the LA method and the smooting method are shown in Table 9 (The smoothing transition consists of 20 pixels).

ERDA	RMSE	HSM	SMD
sLAR/Method LA	7.2119e-05	5.1769e-05	**7.3299e-05**
sLAR/Method smooth	6.7121e-05	4.4099e-05	**6.5726e-05**

Table 9: *Real data - after applying methods. Compare with special limited-angle reconstruction (sLAR).*

The numbers for the smoothing method are all smaller than the numbers for the LA-method. This indicates the same as beforehand: the smoothing method performs better than the LA-method.

5 Summary

In Section 1 and introduction to the problem is given. Due to shadowing metal bars in the acquisition set-up data is missing at specific sites in the sinogram. This is referred to as a special limited-angle (sLA) sinogram. Artifacts appear in the reconstructions as streaks; both the synchrotron provied ones, our own data-based reconstructions, the reconstructions based on synthetic data and on real data from ERDA. A mathematical model of the missing data, based on the geometry of the experimental set-up was derived to simulate the missing data.

In Section 2 we have quantified the artifacts in the synthetic-data reconstructions by a set of generic image quality measurements. They are applied to simulated data as well as ERDA data prior to handling the artifacts. This provides a numerical comparison between the full-angle sinograms (FAR) and the special limited-angle sinograms (sLAR) where streaks are absent and present, respectively. The measures, RMSE, TSM, and SMD will also be calculated after having applied the artifact reduction methods as a means to evaluate the artifact reduction methods. In this section, also the relation between the singularities in the sinogram and streaks in the image is argued for:

- The number of steps in the sinogram corresponds to the number of streaks in the image.
- The angular position of the step in the sinogram corresponds the the angle of the streak in the image.

This study states that treaks are present due to singularities in the sinogram. The boundary of the missing data, bd(A) gives rise to streaks in the image if: a) bd(A) is not smooth or b) if there are singularities in the data at the bd(A) for LA-data ([5]).

Knowing the cause of the streaks, makes it possible to use methods to remove them. Two methods are presented in Section 3: The LA-method and local smoothing:

- LA: This method sets all truncated projection to zero, thereby turning the sinogram into a regular limited-angle sinogram. By doing this we get rid of the detector directed edges. However, we still have edges in the angular direction causing artifacts. These artifacts are not as pronounced, though, since they scale with the differences in the image on the boundary.
- Smoothing: This method performs local smoothing of the detector directed edges by use of a function that attenuates the function values in the sinogram in a smooth way until the region where the value of zero is reached.

After having applied the methods, the reconstructions in Section 4 illustrates that the streaks are removed by either of the methods. Comparison of the two methods shows that local smoothing outperforms the LA-method.

6 Discussion

The presented methods for artifact removal works satisfactory and the reconstructions can be used for subsequent void/material segmentation. During this work, a lot of other methods have been investigated. It seems that the dataset is rather easy to work with since many approaches seems fruitful. The problem resembles regular metal artifact problems, which are rather well studied, but this problem the metal bars are outside the material.

This study only includes preprocessing of the sinogram prior to use of FBP. Algebraic methods are more complicated for ROI-data and are therefore not included in this study.

Future work includes quantification of improvents on a large number of datasets and testing the methods on problems where metal is inside the material instead of outside.

7 Acknowledgements

In want to thank Jon Sporring, Jürgen Frikel, Todd Quinto, and Franǫis Lauze for many and extensive discussions on the topics in this report.

References

[1] P. M. Joseph and R. D Spital. The exponential edge-gradient effect in x-ray computed tomography, Phys. Med Biol, vol 26, no. 3, 473487, 1981

[2] Natterer, F., The Mathematics of Computerized Tomography. Society for Industrial and Applied Mathematics, Phildelphia, PA, USA, 2001.

[3] Kanters, F., Towards Object-based Image Editing, p. 60-63. PrintPartners Ipskamp, Enschede, The Netherlands, 2006.

[4] Bian, J. et al., *Evaluation of sparse-view reconstruction from flat-panel-detector cone-beam CT*, Phys. Med. Biol. **55** (2010), no. 3, 6575–6599.

[5] Frikel, J., E.T. Quinto, *Characterization and reduction of artifacts in limited angle tomography*, *Inverse Problems*, 29(12), 2013.